Thermoelectric coefficients of *n*-doped silicon from first principles via the solution of the Boltzmann transport equation

Mattia Fiorentini and Nicola Bonini*
Department of Physics, King's College London, Strand, London WC2R 2LS, United Kingdom
(Received 1 June 2016; revised manuscript received 1 August 2016; published 25 August 2016)

We present a first-principles computational approach to calculate thermoelectric transport coefficients via the exact solution of the linearized Boltzmann transport equation, also including the effect of nonequilibrium phonon populations induced by a temperature gradient. We use density functional theory and density functional perturbation theory for an accurate description of the electronic and vibrational properties of a system, including electron-phonon interactions; carriers' scattering rates are computed using standard perturbation theory. We exploit Wannier interpolation (both for electronic bands and electron-phonon matrix elements) for an efficient sampling of the Brillouin zone, and the solution of the Boltzmann equation is achieved via a fast and stable conjugate gradient scheme. We discuss the application of this approach to *n*-doped silicon. In particular, we discuss a number of thermoelectric properties such as the thermal and electrical conductivities of electrons, the Lorenz number and the Seebeck coefficient, including the phonon drag effect, in a range of temperatures and carrier concentrations. This approach gives results in good agreement with experimental data and provides a detailed characterization of the nature and the relative importance of the individual scattering mechanisms. Moreover, the access to the exact solution of the Boltzmann equation for a realistic system provides a direct way to assess the accuracy of different flavors of relaxation time approximation, as well as of models that are popular in the thermoelectric community to estimate transport coefficients.

DOI: 10.1103/PhysRevB.94.085204

I. INTRODUCTION

A detailed understanding of electrical transport and energy dissipation phenomena is crucial for the discovery and the development of high-performance materials and devices for applications ranging from nanoelectronics to energy conversion technologies. For this, there is nowadays a growing demand for accurate and efficient computational tools to compute electrical transport coefficients from first principles [1]. The challenge here is a proper description of the dynamics of carriers, while accounting for the relevant carriers' scattering mechanisms. In this context, the Boltzmann transport equation (BE) offers a convenient framework for a detailed microscopic description of transport in metals and semiconductors. However, achieving the full predictive power of this theory requires the exact solution of the BE that is a complex integrodifferential equation, as well as accurate materials' parameters, including electronic band structures and electron-phonon and electron-defect scattering terms.

Different flavors of relaxation-time approximation are often used to tackle the complexity of the BE, but their accuracy in predicting the changes of properties with temperature or carrier concentration is not always satisfactory; for instance, Xu and Verstraete [2] have recently shown that the constant relaxation-time approximation, a popular and quite successful scheme to estimate electronic transport coefficients, provides qualitatively wrong results for the Seebeck coefficient of a relatively simple system such as bulk lithium.

Only in recent years the first efforts have been put forward to solve numerically the BE beyond the relaxation-time approximation and using *ab initio* materials' parameters. For instance, Wang and coworkers [3] computed the thermoelectric properties of *n*-doped silicon from the numerical solution of the linearized Boltzmann equation where the electronic band structure and average intervalley deformation potentials were computed from first-principles, while semiempirical models were used for intravalley scattering, charged impurity scattering and electron-plasmon coupling. In a more recent work, Li [4] studied the transport properties of *n*-doped Si, Al, and *n*-doped MoS_2 by solving the linearized BE using a standard iterative technique and including *ab initio* bands and electron-phonon scattering obtained from a linear interpolation of the *ab initio* electron-phonon matrix elements computed on a coarse grid. Despite these advances, the calculation of thermoelectric transport properties fully from-first-principles still represents a challenge, even in the case of simple metals or semiconductors.

In this paper, we present a first-principles computational infrastructure to calculate electrical transport coefficients of materials from the exact solution of the linearized BE. We use density functional theory (DFT) and density functional perturbation theory (DFPT) for an accurate description of the electronic and vibrational properties of a system, including electron-phonon interactions; carriers' scattering rates are computed using standard perturbation theory. We exploit Wannier interpolation [5,6] for both electronic bands and electron-phonon matrix elements for an efficient sampling of the Brillouin zone, and the solution of the Boltzmann equation is achieved via a fast and stable conjugate gradient scheme.

We discuss the application of this general methodology to *n*-doped silicon. In particular, we discuss a number of thermoelectric properties such as thermal and electrical conductivities of electrons, Seebeck coefficient and Lorenz number in a range of temperatures and donor concentrations, also including the effects related to nonequilibrium phonon populations induced by a temperature gradient.

*nicola.bonini@kcl.ac.uk

Silicon represents an excellent test case to validate our approach as its electronic transport properties have been extensively studied in the past. In particular, there are several theoretical works focusing on transport coefficients of silicon computed using semiempirical models (see, for instance, Ref. [7]) as well as using *ab initio* scattering terms within the relaxation time approximation [8–11] or within the exact solution of the BE [3,4]. In addition to this, the role of the coupled electron-phonon dynamics on the thermoelectric properties of silicon has very recently attracted renewed interest [11–13]. Indeed, in this material there is a substantial enhancement, even at room temperature and in heavily doped samples, of the Seebeck coefficient induced by the drag exerted on charge carriers from phonons diffusing along a temperature gradient (phonon drag). In the past, this topic has not received much attention beyond the initial experimental [14] and theoretical [15] works, but with current interest in thermoelectric energy conversion this effect might represent an interesting route to enhance thermoelectric performance [11].

The structure of the paper is as follows. In the Sec. II, we present the theoretical framework for transport. The results for the transport coefficients on n-doped silicon are presented and discussed in Sec. III. The details of the BE solver, the convergence and the performance of the numerical techniques are discussed in the appendices.

II. METHODOLOGY

A. Boltzmann transport in linear response

When an electric field $\boldsymbol{E}$ and a temperature gradient $\nabla_{\boldsymbol{r}} T$ are present across a material, the steady-state distribution function $f_m(\boldsymbol{k})$ of charge carriers at band m and wave vector $\boldsymbol{k}$ can be described by the BE [16]

$$\boldsymbol{v}_{m\boldsymbol{k}} \cdot \nabla_{\boldsymbol{r}} T \frac{\partial f_m(\boldsymbol{k})}{\partial T} - \frac{e}{\hbar} \boldsymbol{E} \cdot \nabla_{\boldsymbol{k}} f_m(\boldsymbol{k}) = \left(\frac{\delta f_m(\boldsymbol{k})}{\delta t} \right)_{\text{coll}}, \quad (1)$$

where e is the electronic charge, $\boldsymbol{v}_{m\boldsymbol{k}} = \nabla_{\boldsymbol{k}} \epsilon_{m\boldsymbol{k}}/\hbar$ is the electron velocity (where $\epsilon_{m\boldsymbol{k}}$ is the quasiparticle energy). The term on the right is the collision term given by

$$\left(\frac{\delta f_m(\boldsymbol{k})}{\delta t} \right)_{\text{coll}} = \frac{1}{N_{\boldsymbol{k}}} \sum_{m'\boldsymbol{k}'} \{ f_{m'}(\boldsymbol{k}') W_{m'\boldsymbol{k}' \to m\boldsymbol{k}} [1 - f_m(\boldsymbol{k})] - f_m(\boldsymbol{k}) W_{m\boldsymbol{k} \to m'\boldsymbol{k}'} [1 - f_{m'}(\boldsymbol{k}')] \},$$

where $N_{\boldsymbol{k}}$ is the number of k points in the Brillouin zone (BZ) and $W_{m\boldsymbol{k} \to m'\boldsymbol{k}'}$ is the probability per unit time for an electron in a state m, $\boldsymbol{k}$ to be scattered into an empty state m', $\boldsymbol{k}'$ (the details of $W_{m\boldsymbol{k} \to m'\boldsymbol{k}'}$ for the different scattering mechanisms are given in Sec. II B).

If the external fields are weak, it is possible to write the steady-state distribution in terms of the equilibrium one, $f^0_m(\boldsymbol{k})$, and a term that is linear in the perturbing fields,

$$f_m(\boldsymbol{k}) = f^0_m(\boldsymbol{k}) - \frac{\partial f^0_m(\boldsymbol{k})}{\partial \epsilon_{m\boldsymbol{k}}} \chi_m(\boldsymbol{k}). \quad (2)$$

In this way, it is possible to derive the linearized Boltzmann equation that can be solved to obtain $\chi_m(\boldsymbol{k})$,

$$-\frac{\partial f^0_m(\boldsymbol{k})}{\partial \epsilon_{m\boldsymbol{k}}} \boldsymbol{v}_{m\boldsymbol{k}} \cdot \left[\boldsymbol{E} e + \frac{\nabla_{\boldsymbol{r}} T}{T} (\epsilon_{m\boldsymbol{k}} - \mu) \right] = \frac{1}{k_B T N_{\boldsymbol{k}}} \sum_{m'\boldsymbol{k}'} \Pi^0_{m'\boldsymbol{k}', m\boldsymbol{k}} [\chi_{m'}(\boldsymbol{k}') - \chi_m(\boldsymbol{k})], \quad (3)$$

where μ is the chemical potential and we have used $\Pi^0_{m'\boldsymbol{k}', m\boldsymbol{k}} = f^0_{m'}(\boldsymbol{k}')[1 - f^0_m(\boldsymbol{k})] W_{m'\boldsymbol{k}' \to m\boldsymbol{k}}$. This equation can be written in the matrix form $\boldsymbol{b} = \boldsymbol{A}\boldsymbol{x}$, where $\boldsymbol{b}$ is the left-end side of Eq. (3), $\boldsymbol{x} = \chi_m(\boldsymbol{k})$ and the matrix $\boldsymbol{A}$ is

$$A_{i'i} = \frac{1}{k_B T N_{\boldsymbol{k}}} \left[\Pi^0_{i'i} - \delta_{i'i} \sum_{i''} \Pi^0_{i''i} \right],$$

where $i = \{m, \boldsymbol{k}\}$. $\boldsymbol{A}$ is symmetric and positive semidefinite [16].

The expressions for the charge current $\boldsymbol{j}_e$ and the heat current $\boldsymbol{j}_\epsilon$ are

$$\boldsymbol{j}_e = \frac{2e}{V N_{\boldsymbol{k}}} \sum_{m\boldsymbol{k}} \boldsymbol{v}_{m\boldsymbol{k}} \frac{\partial f^0_m(\boldsymbol{k})}{\partial \epsilon_{m\boldsymbol{k}}} \chi_m(\boldsymbol{k}), \quad (4a)$$

$$\boldsymbol{j}_\epsilon = -\frac{2}{V N_{\boldsymbol{k}}} \sum_{m\boldsymbol{k}} (\epsilon_{m\boldsymbol{k}} - \mu) \boldsymbol{v}_{m\boldsymbol{k}} \frac{\partial f^0_m(\boldsymbol{k})}{\partial \epsilon_{m\boldsymbol{k}}} \chi_m(\boldsymbol{k}), \quad (4b)$$

where V is the volume of the unit cell. In linear response, the electric and thermal current densities are related to the external fields via *transport coefficients*

$$\boldsymbol{j}_e = \sigma \left[\boldsymbol{E} + S T \left(-\frac{\nabla_{\boldsymbol{r}} T}{T} \right) \right], \quad (5a)$$

$$\boldsymbol{j}_\epsilon = \alpha \boldsymbol{E} + \beta T \left(-\frac{\nabla_{\boldsymbol{r}} T}{T} \right). \quad (5b)$$

It has to be remarked that in this formalism $\boldsymbol{E} = \nabla_{\boldsymbol{r}}(\phi - \mu/e)$ is the effective electric field arising from both an electric and chemical potential gradient and should be regarded as the *electrochemical* field. Also, in principle, the transport coefficients are tensors [17], but they are scalars in the case of silicon.

The quantities on which we will focus on for n-doped silicon are the electrical resistivity $\rho_e = 1/\sigma$ (where σ is the electrical conductivity), the electron mobility $\mu_e = \sigma/en$ (where n is the carrier concentration), the Seebeck coefficient S, and the Lorenz number $L = \mathscr{K}_e/\sigma T$ (where $\mathscr{K}_e = \beta - \alpha S$ is the thermal conductivity of the electrons).

In order to establish a link with the relaxation-time approximation, it is possible to rewrite $\chi_m(\boldsymbol{k})$ in this way:

$$\chi_m(\boldsymbol{k}) = -\boldsymbol{v}_{m\boldsymbol{k}} \cdot \left[\boldsymbol{E} e \tau^e_m(\boldsymbol{k}) + \frac{\nabla_{\boldsymbol{r}} T}{T} (\epsilon_{m\boldsymbol{k}} - \mu) \tau^t_m(\boldsymbol{k}) \right], \quad (6)$$

where we have introduced two effective *transport* relaxation times $\tau^e_m(\boldsymbol{k})$ and $\tau^t_m(\boldsymbol{k})$ that are determined from the solution of the BE's that include only the electric field and only the thermal gradient, respectively. With this definition, the

transport coefficients have familiar forms [18]:

$$\sigma = -\frac{2e^2}{VN_{\boldsymbol{k}}}\sum_{m\boldsymbol{k}}\frac{\partial f^0_m(\boldsymbol{k})}{\partial\epsilon_{m\boldsymbol{k}}}[v^{||}_m(\boldsymbol{k})]^2\tau^e_m(\boldsymbol{k}), \tag{7a}$$

$$\sigma S = \frac{2e}{TVN_{\boldsymbol{k}}}\sum_{m\boldsymbol{k}}\frac{\partial f^0_m(\boldsymbol{k})}{\partial\epsilon_{m\boldsymbol{k}}}[v^{||}_m(\boldsymbol{k})]^2(\epsilon_{m\boldsymbol{k}}-\mu)\tau^t_m(\boldsymbol{k}), \tag{7b}$$

$$\alpha = \frac{2e}{VN_{\boldsymbol{k}}}\sum_{m\boldsymbol{k}}\frac{\partial f^0_m(\boldsymbol{k})}{\partial\epsilon_{m\boldsymbol{k}}}[v^{||}_m(\boldsymbol{k})]^2(\epsilon_{m\boldsymbol{k}}-\mu)\tau^e_m(\boldsymbol{k}), \tag{7c}$$

$$\beta = -\frac{2}{TVN_{\boldsymbol{k}}}\sum_{m\boldsymbol{k}}\frac{\partial f^0_m(\boldsymbol{k})}{\partial\epsilon_{m\boldsymbol{k}}}[v^{||}_m(\boldsymbol{k})]^2(\epsilon_{m\boldsymbol{k}}-\mu)^2\tau^t_m(\boldsymbol{k}), \tag{7d}$$

where $v^{||}_m(\boldsymbol{k})$ is the component of the velocity along the applied field.

B. Sources of electronic scattering

The main ingredients that determine the transport characteristics of a material are the transition probabilities per unit time, $W_{m\boldsymbol{k}\to m'\boldsymbol{k}'}$ on the right-hand side of Eq. (3). Below, we discuss the transition probabilities for the sources of electronic scattering that we used to simulate the transport properties of n-doped silicon.

1. Electron-phonon coupling

Under the assumption that lattice vibrations are in thermal equilibrium, the transition probability due to electron-phonon scattering is given by [16]

$$\begin{aligned}W^{\text{el-ph}}_{m\boldsymbol{k}\to m'\boldsymbol{k}+\boldsymbol{q}} = \frac{2\pi}{\hbar}\sum_{\lambda}\left|g^{\lambda}_{mm'}(\boldsymbol{k};\boldsymbol{q})\right|^2 \\ \times\left\{n^0_{\lambda}(\boldsymbol{q})\,\delta[\epsilon_{m'\boldsymbol{k}+\boldsymbol{q}}-\epsilon_{m\boldsymbol{k}}-\hbar\omega_{\lambda}(\boldsymbol{q})]\right. \\ \left.+\left[n^0_{\lambda}(\boldsymbol{q})+1\right]\delta[\epsilon_{m'\boldsymbol{k}+\boldsymbol{q}}-\epsilon_{m\boldsymbol{k}}+\hbar\omega_{\lambda}(\boldsymbol{q})]\right\},\end{aligned} \tag{8}$$

where $\omega_{\lambda}(\boldsymbol{q})$ and $n^0_{\lambda}(\boldsymbol{q})$ are the phonon frequency and the equilibrium distribution of the phonon mode of branch index λ and wave vector $\boldsymbol{q}$, and the electron-phonon matrix elements are given by

$$g^{\lambda}_{mm'}(\boldsymbol{k};\boldsymbol{q}) = \sqrt{\frac{\hbar}{2M\omega_{\lambda}(\boldsymbol{q})}}\,\langle m\boldsymbol{k}+\boldsymbol{q}|\partial_{\lambda\boldsymbol{q}}V|m'\boldsymbol{k}\rangle\,, \tag{9}$$

where $|m'\boldsymbol{k}\rangle$ and $|m\boldsymbol{k}+\boldsymbol{q}\rangle$ are the Bloch eigenstates, M is the atomic mass, and $\partial_{\lambda\boldsymbol{q}}V$ is the derivative of the Kohn-Sham self-consistent potential with respect to the atomic displacement corresponding to a phonon mode λ at $\boldsymbol{q}$.

2. Ionized impurities

Even though it is nowadays possible to compute form first-principles the interaction between charge carriers and ionized impurities in semiconductors [8,19], in this work we rely on a simple analytical model developed by Brooks and Herring (BH) [7]. In this model, the transition probability per unit time is given by

$$W^{\text{el-imp}}_{m\boldsymbol{k}\to m'\boldsymbol{k}+\boldsymbol{q}} = \frac{2\pi Z^2 n_i e^4}{\hbar V_{ws}(\epsilon_r\epsilon_0)^2}\frac{\delta(\epsilon_{m'\boldsymbol{k}+\boldsymbol{q}}-\epsilon_{m\boldsymbol{k}})}{\left(\beta_s{}^2+|\boldsymbol{q}|^2\right)^2}, \tag{10}$$

where Ze is the charge of the impurity, n_i is the impurity density, ϵ_r and ϵ_0 are the relative and the vacuum permittivity. In the Debye approach [20], for nondegenerate semiconductors, the reciprocal of the screening length β_s is given by

$$\beta_s = \sqrt{\frac{e^2 n_i}{\epsilon_r\epsilon_0 k_B T}}. \tag{11}$$

In this work, we focus on n-doped silicon and assume that all the donor impurities are completely ionized, i.e., the donor density is equal to the free carriers' concentration.

C. Phonon drag

The assumption of thermal equilibrium of the lattice is not strictly valid anymore when a temperature gradient is present across a material. In this case, nonequilibrium phonon populations can leave a fingerprint on the thermoelectric coefficients. This effect was first predicted by Gurevich in 1945 [21], and, only later, experiments on germanium [22,23] and silicon [14] clearly revealed the related *anomalous* peak in the Seebeck coefficient at low temperatures.

In order to accurately account for this effect, in principle, one should solve the coupled BE's for the electrons and phonons. An alternative approach to this computationally demanding effort was proposed by Cantrell *et al.* [24] in the context of a relaxation time approximation and it exploits the possibility to partially decouple the electron and phonon transport for weak electron-phonon coupling. This approach has been recently implemented and used in silicon within an *ab initio* framework [11]. In this work, we proceed along a similar line but in the context of the exact solution of the BE. In particular, we partially decouple the two BE equations under the assumption that the nonequilibrium phonon populations that arise in presence of a temperature gradient can be computed neglecting the electron-phonon scattering in the BE for phonons. This approximation is reasonable in silicon at carriers' concentration lower than 10^{19} cm^{-3} as in this regime the thermal conductivity is the same as in undoped silicon [25]. In this way, it is possible to compute the steady-state correction to the equilibrium phonon populations, $\delta n_{\lambda}(\boldsymbol{q})$, from the BE for phonons, and include them into the full BE for the electrons. By considering only the first order deviation of the distribution functions, it is possible to obtain [12] a linearized BE for electrons that is the same as Eq. (3) apart an additional term on the left-hand side given by

$$\begin{aligned}\left(\frac{\delta f_m(\boldsymbol{k})}{\delta t}\right)_{\text{Ph drag}} = -\frac{2\pi}{\hbar}\sum_{\lambda,\boldsymbol{q}m'}\left|g^{\lambda}_{mm'}(\boldsymbol{k};\boldsymbol{q})\right|^2 \\ \times\{\delta n_{\lambda}(\boldsymbol{q})\,\delta[\epsilon_{m'\boldsymbol{k}+\boldsymbol{q}}-\epsilon_{m\boldsymbol{k}}-\hbar\omega_{\lambda}(\boldsymbol{q})] \\ +\delta n_{\lambda}(-\boldsymbol{q})\,\delta[\epsilon_{m'\boldsymbol{k}+\boldsymbol{q}}-\epsilon_{m\boldsymbol{k}}+\hbar\omega_{\lambda}(\boldsymbol{q})]\} \\ \times\left[f^0_{m'}(\boldsymbol{k}+\boldsymbol{q})-f^0_m(\boldsymbol{k})\right].\end{aligned} \tag{12}$$

This term is the driving force that is responsible for an additional electrical current in the same direction as the heat

flow, as if the charge carriers were dragged along by phonons. This effect results in a *phonon drag* contribution to the Seebeck effect that adds to the standard *diffusive* part. In this work, we compute $\delta n_\lambda(\boldsymbol{q})$ using the single-mode relaxation time approximation

$$\delta n_\lambda(\boldsymbol{q}) = -\tau_\lambda(\boldsymbol{q})\frac{\boldsymbol{c}_\lambda(\boldsymbol{q})\cdot\nabla_r T}{k_B T^2}\hbar\omega_\lambda(\boldsymbol{q})n^0_\lambda(\boldsymbol{q})\left[n^0_\lambda(\boldsymbol{q})+1\right], \tag{13}$$

where $\tau_\lambda(\boldsymbol{q})$, $\boldsymbol{c}_\lambda(\boldsymbol{q})$ are the anharmonic phonon lifetime and the group velocity of the phonon mode λ at $\boldsymbol{q}$, respectively.

D. Computational details

We used DFT and DFPT as implemented in the QUANTUM ESPRESSO distribution [26] within the local-density approximation (LDA) [27] to compute the electronic and vibrational properties including the electron-phonon coupling matrix elements. We used a norm-conserving pseudopotential and a plane-wave expansion up to a 30 Ry cutoff. Brillouin zone sampling was performed on $12\times12\times12$ Monkhorst-Pack mesh for all charge density and phonon calculations. We used a theoretical lattice parameter of 5.41 Å. All the quantities $\epsilon_{m\boldsymbol{k}}$, $\boldsymbol{v}_{m\boldsymbol{k}}$, and $g^\lambda_{mm'}(\boldsymbol{k};\boldsymbol{q})$ have been first calculated on grids of $10\times10\times10$ k-points and $5\times5\times5$ q points. Then we have used a first-principles interpolation scheme [6] based on maximally localized Wannier functions [5], as implemented in the WANNIER90 [28] and EPW [29] packages to compute transport quantities on very dense meshes up to $110\times110\times110$. Wannier interpolation has been used successfully in recent works on the electrical transport properties of graphene [30], phosphorene [31], silicon [11], and bulk metals [32].

Even though the Wannier interpolation of the electron-phonon matrix elements is computationally efficient, it is quite time consuming when many k points are required to achieve converged transport coefficients. To reduce the computational burden, we have adopted a double grid scheme, in which the electron-phonon coupling matrix elements computed via Wannier interpolation are stored on a fine mesh in reciprocal space ($N_{\mathrm{EPC}}\times N_{\mathrm{EPC}}\times N_{\mathrm{EPC}}$), and an ultra fine grid ($N_f\times N_f\times N_f$, with $N_f = p\cdot N_{\mathrm{EPC}}$ and $p = 1,2,3$) is used to solve the BE and compute the transport quantities. For the points in the ultrafine grid, we only compute electronic bands and phonon frequencies, and use the electron-phonon matrix elements at the closest points in the $N_{\mathrm{EPC}}\times N_{\mathrm{EPC}}\times N_{\mathrm{EPC}}$ grid. This choice is motivated by the fact that the electron-phonon matrix elements are a rather smooth function in the Brillouin zone while the transition probabilities (involving delta functions and products of distribution functions) exhibit a more oscillatory behavior. The delta functions in the transition probabilities are replaced with Gaussians. Converged transport properties were obtained with $N_{\mathrm{EPC}} = 70$, $p = 3$ and a Gaussian width of 4 meV. Doping has been simulated within the rigid band approximation via a shift of the chemical potential. The convergence of the transport properties with respect to the grids and Gaussian width is discussed in Appendix B. The solution of the BE is achieved with an in-house parallel code that uses a fast and stable preconditioned conjugate gradient (CG) algorithm [33]. A similar approach has been used for the solution of the BE for phonons by Fugallo *et al.* [34].

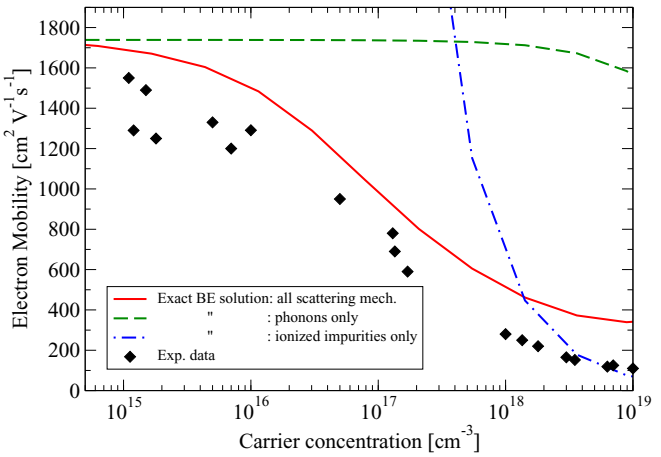

FIG. 1. Electron mobility as a function of carrier concentration at $T = 300$ K. The solid red line is obtained by solving the BE that includes both impurity and phonon scattering. The dashed green line (dot-dashed blue line) is from the solution of the BE with just phonon (charged impurity) scattering. The experimental data are taken from Ref. [37].

Appendix A discusses the accuracy and the performance of the BE solver.

The anharmonic phonon lifetimes needed to compute the contribution of the phonon drag to the transport coefficients were computed within the single mode relaxation time approximate and from the third-order force constants used in Refs. [35,36]. In this work, we have recalculated the lifetimes on a $(70\times70\times70)$ mesh of q points using a Gaussian width of 0.25 meV.

III. RESULTS

A. Mobility and resistivity

In Figs. 1 and 2, we present our results for the electron mobility of n-doped silicon. The room temperature results

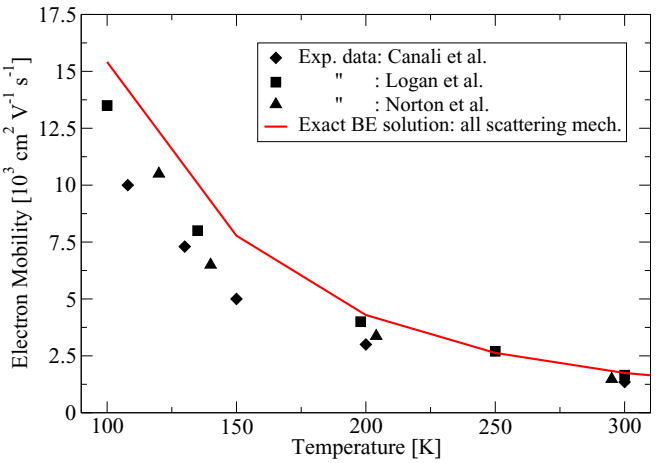

FIG. 2. Electron mobility as a function temperature at $n = 10^{14}$ cm^{-3}. The solid red line is obtained from the solution of the BE. The experimental data are from Canali *et al.* [40] (diamonds), Logan *et al.* [41] (squares), and Norton *et al.* [42] (triangles).

(Fig. 1) show that for carrier concentrations lower than 10^{15} cm^{-3}, the mobility is mainly limited by electron-phonon interactions; at higher carriers concentrations, instead, the mobility decreases as a result of an increased electron-impurity scattering. As the temperature increases the mobility decreases (Fig. 2) mainly because of a stronger electron-phonon scattering. Our predicted electron mobility is in reasonable agreement with the reported experimental data as a function of doping and temperature. It is however clear that our results tend to overestimate the experimental results (but note that the uncertainty in the experimental data is quite large, around 10% at low doping). This could be related to an underestimation of the electron-phonon coupling computed within standard DFT at the level of LDA. Indeed, similar shortcomings of LDA have been reported quite recently for other materials, including simple sp-bonded compounds, such as graphene [30] and diamond [38]. It is important to point out that the discrepancy at high doping with the experimental data could also be related to additional scattering mechanisms involving electron-plasmon interactions [39] that we have not included in this work.

It is interesting to compare our results with previous DFT-based theoretical work. Focussing on the room temperature, low-doping regime, our prediction for the phonon-limited mobility is 1750 $cm^2\,V^{-1}\,s^{-1}$. Our result is slightly closer to experiments than the value of 1860 $cm^2\,V^{-1}\,s^{-1}$ reported in Ref. [4], where the BE is numerically solved. This difference is probably related to the different interpolation schemes (Wannier versus linear interpolation) of the electron-phonon matrix elements and the result of a different sampling of the BZ. The comparison with DFT-based results obtained within the relaxation time approximation shows that our result is somehow in between the reported values of 1970 $cm^2\,V^{-1}\,s^{-1}$ (see Ref. [8]) and around 1550 $cm^2\,V^{-1}\,s^{-1}$ (see Ref. [11]). While the discrepancies with respect to Ref. [8] could be related to a different sampling of the BZ, it is not easy to identify the origin of the differences with the results of Ref. [11], in which both the interpolation scheme and the k-point grids used are very close to the ones used in this work. However, it is interesting to point out that, as shown in Appendix C, the use of the relaxation time approximation as in Ref. [11] gives electron mobilities that are 4%–5% lower than the prediction from the exact solution of the BE, making the discrepancy between the two works slightly less pronounced.

It is interesting at this point to analyze in more detail the contribution of the different scattering channels to the electrical transport. As shown in Fig. 1, information about the role of different mechanisms can be obtained switching on and off interactions when solving the BE. This analysis, however, is only qualitative as the effects are not additive. In order to provide a quantitative estimate of the contributions from the different scattering channels, a possibility is to focus on the electrical resistivity and exploit the variational formula [16]

$$\rho_e = \frac{V}{4e^2 k_B T} \frac{\sum_{m\boldsymbol{k},m'\boldsymbol{k}'} [\chi_m(\boldsymbol{k}) - \chi_{m'}(\boldsymbol{k}')]^2 \Pi^0_{m\boldsymbol{k},m'\boldsymbol{k}'}}{\left[\sum_{m\boldsymbol{k}} v^{||}_m(\boldsymbol{k}) \chi_m(\boldsymbol{k}) \frac{\partial f^0_m(\boldsymbol{k})}{\partial \epsilon_{m\boldsymbol{k}}}\right]^2}. \quad (14)$$

This formula has its minimum value (the steady-state electrical resistivity) when $\chi_m(\boldsymbol{k})$ is the solution of the BE, and it is often used to determine an upper bound to the resistivity when using trial functions. In this case, however, we insert in Eq. (14) the solution of the BE and exploit the fact that in Eq. (14) the different contributions from the scattering mechanisms are additive. The electrical resistivity at room temperature is shown in Fig. 3: our results reproduce well the experimental data as a function of carrier concentration. In Fig. 4, we present the results of the analysis based on Eq. (14) of the different contributions to the resistivity in the low- and high-doping regimes. At low doping, the role of impurities is negligible and the main contribution (around 55%) comes from intravalley acoustic phonon scattering. The remaining 45% is from intervalley transitions. It is interesting to observe that around 35% of these contributions are due to scattering with intervalley optical phonon modes. At higher doping (in a regime in which screening effects are weak), charged impurity scattering becomes dominant, accounting for almost 70% of the resistivity. Intervalley channels also increase their importance relatively to intravalley ones.

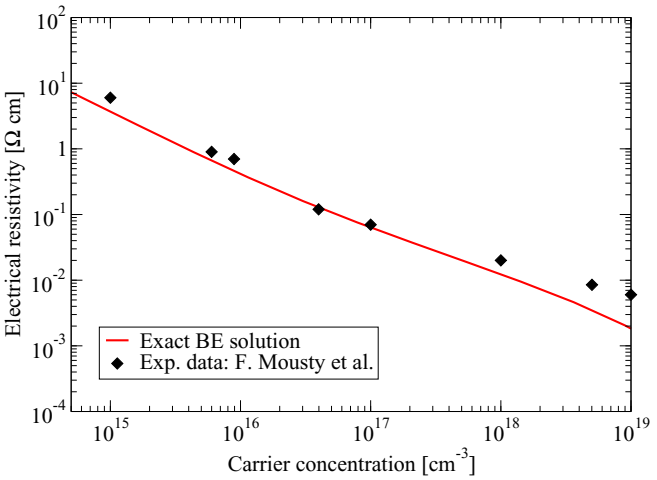

FIG. 3. Electrical resistivity as a function of carrier concentration at $T = 300$ K. Experimental data from Ref. [43].

B. Seebeck coefficient

Figure 5 shows the theoretical results for the Seebeck coefficient as a function of carrier concentration at $T = 300$ K. The diffusive part of S is the largest contribution and determines the overall dependence on the carrier concentration. The phonon drag adds up a nearly constant term that contributes around 25% of the total S at $T = 300$ K.

At low doping, our results slightly underestimate the measured S but the overall agreement between theory and experiment is good. The underestimation could be due to the fact that (i) the out-of-equilibrium phonon populations that produce the phonon drag have been calculated using the single-mode relaxation time approximation and anharmonic force constants computed on a $3 \times 3 \times 3$ supercell that tend to underestimate the lattice thermal conductivity [36] and (ii) as already mentioned, our calculations seem to slightly underestimate the strength of the electron-phonon coupling.

At very high doping, for $n \gtrsim 10^{19}$ cm^{-3}, our results are higher than the experimental data. This is due to the fact that we

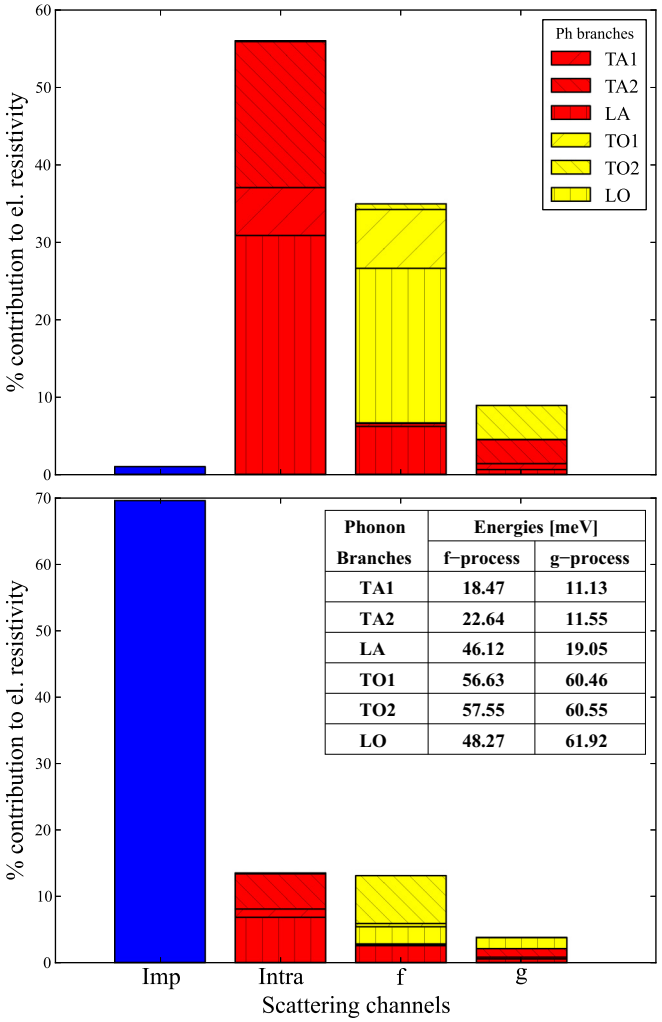

FIG. 4. Relative contribution of the different scattering mechanisms to electrical resistivity at $T = 300$ K. Carriers' concentrations are 2.4×10^{14} (upper panel) and 1.3×10^{19} cm^{-3} (lower panel). The charged impurities' contribution (Imp), intra-valley phonon scattering (Intra) and intervalley phonon scattering (f and g stand for f processes and g processes, described in Ref. [20]) are shown. The phonon scattering are separated in acoustic (dark red) and optical (light yellow) branches, and different patterns are used for the modes: diagonal lines for TA1 and TO1, dense diagonal lines for TA2 and TO2 and vertical lines for LA and LO. The phonon energies of the different modes are also shown.

do not include the additional contribution of electron-phonon scattering when computing the out-of-equilibrium phonon populations. As noted in Ref. [11], at high doping, this *saturation effect* [15] of charge carriers on phonons results in a substantial decrease of the phonon drag contribution and the Seebeck coefficient approaches the diffusive part of S.

It is interesting to note that the diffusive part of S agrees quite well with the prediction of the constant relaxation time approximation (CRTA), a popular and often quite successful approximation implemented in codes such as Bolztrap [44] and Boltzwann [45]. The reason for this is that the diffusive part of S depends very little on the nature of the scattering mechanisms. Indeed, as shown in Fig. 5, switching off phonon

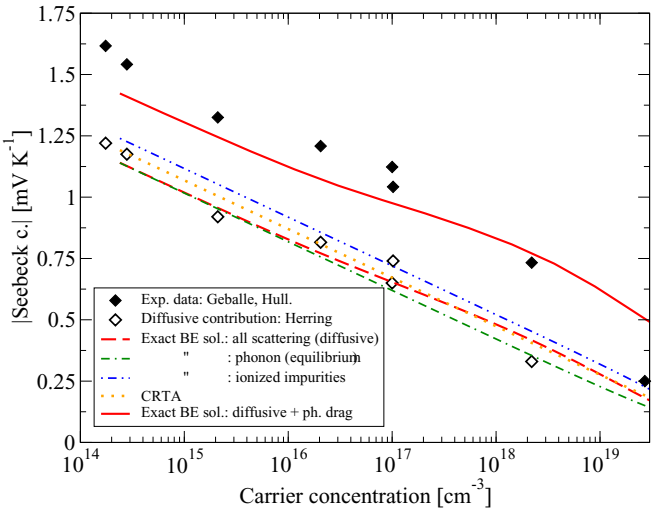

FIG. 5. Seebeck coefficient as a function of carrier concentration at $T = 300$ K. The solid red line is the total Seebeck coefficient, the red dashed line is the diffusive contribution, the orange dotted line is the CRTA result, the green dot-dash-dashed (blue dot-dot-dashed) line is the diffusive S computed including only phonon (impurity) scattering. The solid black diamonds are the experimental results [14], while the open diamonds represent the diffusive Seebeck extracted from the experimental data [14,15].

or impurity scattering when solving the BE affects the result for S by less than 8%.

In order to analyze the contribution of the different phonon modes to the phonon drag part of S, we have solved the BE restricting the term in Eq. (12) to different phonon frequency windows and to specific phonon modes. The results of this analysis are shown in Fig. 6. Our results indicate that low-frequency acoustic phonon modes play a crucial role. For instance, Fig. 6 shows that phonons with frequency below 50 cm^{-1} contribute to about 80% of the phonon drag effect,

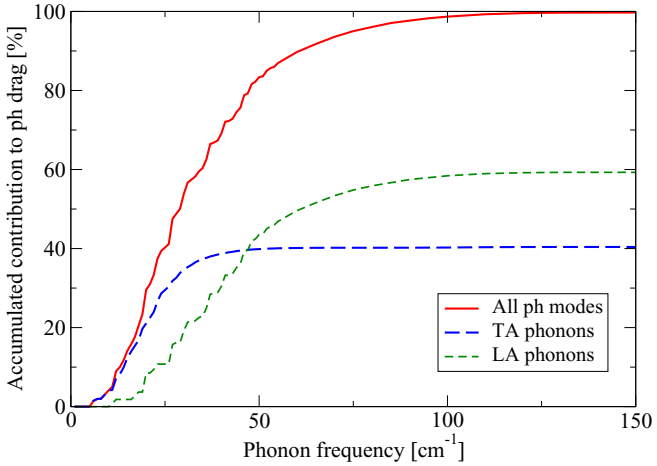

FIG. 6. Contribution of phonon modes to the phonon drag part of the Seebeck coefficient at $T = 300$ K and for $n = 1.75 \times 10^{14}$ cm^{-3}. The solid red line is the contribution from all the modes; the blue long-dashed (green short-dashed) line is the contribution from TA (LA) phonons.

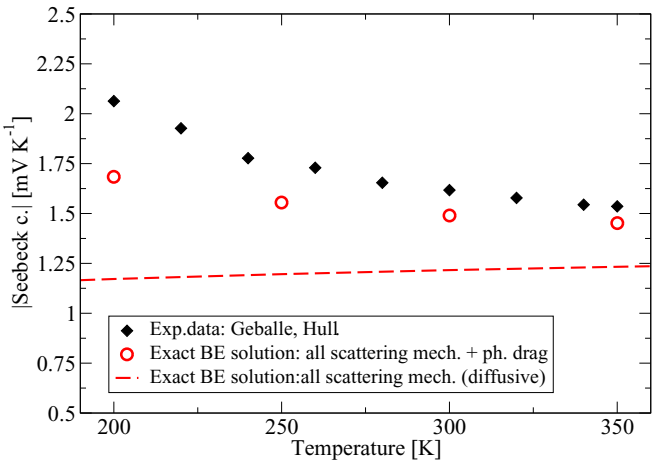

FIG. 7. Seebeck coefficient as a function of temperature for $n = 1.75 \times 10^{14}$ cm^{-3}. The red open circles are the total theoretical Seebeck coefficient while the dashed red line is the diffusive part of S. The black diamonds are the experimental data [14].

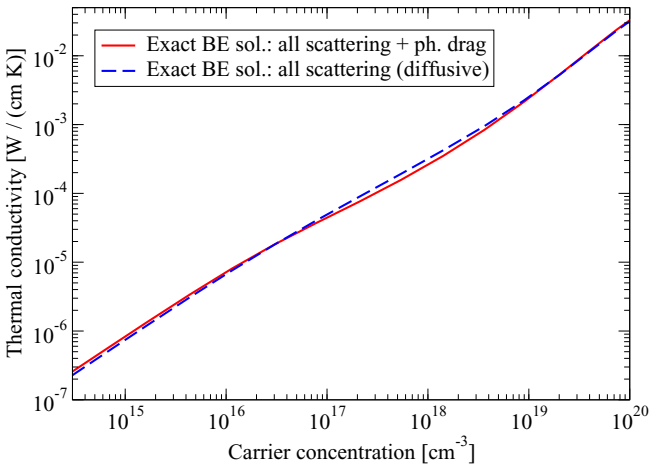

FIG. 8. Electronic thermal conductivity as a function of carrier concentration at $T = 300$ K. The red solid line is from the solution of the BE that includes all the scattering mechanisms and the phonon drag. The blue long-dashed line is the same as the red solid line but without the phonon drag.

with the longitudinal acoustic (LA) modes contributing almost 60% of the total. These data confirm previous findings obtained on the basis of the relaxation-time approximation [11]. As suggested in Ref. [11], an interesting strategy to enhance the zT could be based on a phonon frequency filtering approach. For instance, in silicon at room temperature phonons with frequencies above 50 cm^{-1} contribute to about 80% of the thermal conductivity [11,35]. Engineered scattering of phonons above 50 cm^{-1} could therefore provide an effective way to strongly reduce the thermal conductivity while preserving the beneficial effect of low-frequency phonons on the Seebeck coefficient. This filtering approach could be based on impurity scattering that is typically more effective for phonons at higher frequency (see, for instance, Ref. [35] where this effect has been studied in SiGe alloys). This strategy and, in particular, the possibility to use nanoclusters as impurities is analyzed in more details in Ref. [11].

Figure 7 shows the Seebeck coefficient as a function of temperature at low doping. It is clear that the phonon drag becomes more important at low temperature, resulting in a larger correction to the diffusive S. As Fig. 6 shows, the disagreement between theory and experiment becomes more pronounced at low temperature. This is the result of the fact that the small underestimation that we pointed out for the results at 300 K becomes more marked at lower temperature. In particular, as shown in Ref. [36], our results for the lattice thermal conductivity of silicon show slightly larger deviations at low temperatures. A more accurate estimate of the Seebeck coefficient at low temperature would clearly require a more accurate calculation of phonon transport in silicon, but this is beyond the scope of this work.

C. Lorenz number

The Lorenz number (or Lorenz function) $L = \mathscr{K}_e/\sigma T$ is an important quantity in thermoelectrics research, as it provides a way to separate the electronic thermal and lattice thermal conductivity. Good thermoelectric compounds display a high degree of electronic and structural complexity, and it is not obvious that the Wiedemann-Franz law, derived for simple metals obeying elastic scattering, remains valid also in these compounds. As the design and the optimization of thermoelectric materials involve modifications to the electrical conductivity or lattice thermal conductivity, a precise knowledge of this quantity is important to accurately characterize and compare different compounds and determine successful routes towards higher thermoelectric performance.

The electronic contribution to the thermal conductivity, one of the ingredients to compute L, is shown in Fig. 8. This quantity increases with the carrier concentration, but even at $n = 10^{20}$cm^{-3} the room-temperature electronic thermal

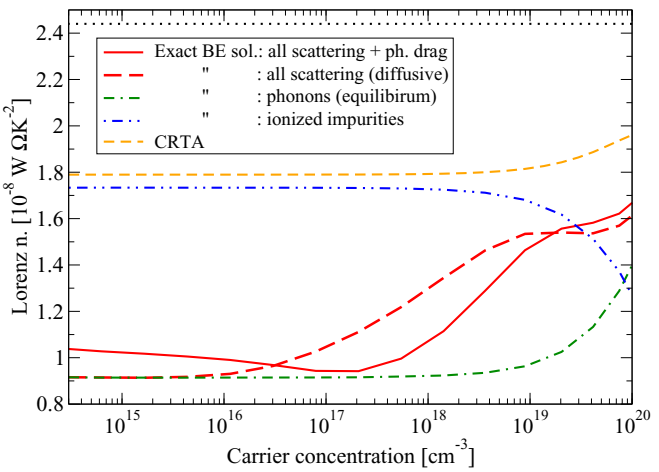

FIG. 9. Lorenz number L as a function of carrier concentration at $T = 300$ K. The red solid line is from the solution of the BE that includes all the scattering mechanisms and the phonon drag. The red long-dashed line is the same as the red solid line but without the phonon drag. The green dot-dash-dashed (blu dot-dot-dashed) line is from the BE including only phonon (impurity) scattering. The orange short-dashed line is the CRTA. The black dotted horizontal line is the Wiedemann-Franz result.

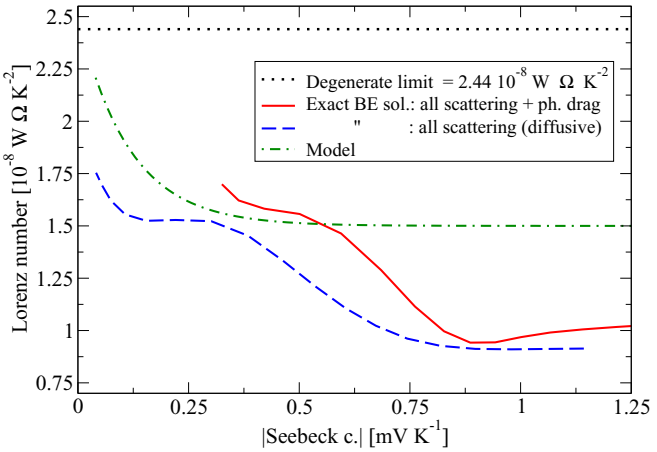

FIG. 10. Lorenz number L as a function of Seebeck coefficient S at $T = 300$ K. The red solid line (dashed blue line) is from the solution of the BE with (without) the phonon drag. The green dot-dashed line is the model proposed in Ref. [48]. The black dotted horizontal line is the Wiedemann-Franz result.

conductivity is only a small fraction (about 2%) of the lattice thermal conductivity of undoped silicon.

In Fig. 9, we show the Lorenz number L at $T = 300$ K as a function of carrier concentration. At low doping, L tends to a constant value of 1.05×10^{-8} WΩ K^{-2}. In the high-doping regime, L increases with the carrier concentration, but, in the range of doping investigated, it is much smaller than the Lorenz number predicted for metallic systems by the Wiedemann-Franz law ($L = 2.44 \times 10^{-8}$ WΩ K^{-2}).

It is interesting to observe that while the Seebeck coefficient depends very little on the nature of the scattering mechanisms, the Lorenz number is instead quite sensitive: for instance, if we focus on the results that do not include the phonon drag, in the low-doping regime, the result obtained accounting for phonon scattering is quite different from the values obtained with impurity scattering or using the CRTA. It is worth pointing out that this dependence on the nature of the scattering terms has also been noticed in the context of a simple model based on a single parabolic band and power law relaxation times [46,47]. The origin of this marked dependence on the scattering mechanisms is the result of the sensitivity of $\mathscr{K}_e$ on the details of the solution of the BE: the $(\epsilon - \eta)^2$ in Eq. (7d) and the αS term accentuate the differences in the solutions of the BE with different scattering mechanisms in a relevant energy window that is much larger than that for S (Fig. 13 clearly shows that the convergence of S is achieved in a energy window much smaller than for L).

The access to the exact solution of the BE for a realistic system allows the assessment of simplified models to extract the Lorenz number from experimental data. For instance, a recent work [48] proposes the use of an equation for L in terms of the experimentally determined S: $L = 1.5 + \exp -\frac{|S|}{116}$ (where L is in 10^{-8} WΩ K^{-2} and S in μV/K). This equation closely reproduces the L obtained with a model that uses a single band with parabolic dispersion and an energy-dependent relaxation time accounting for acoustic phonon scattering. Figure 10 shows the comparison of this model with our results. At low S up to about 0.6 mV K^{-1}, a range for S that is typical of good thermoelectrics, the model is not too far from the exact result and it certainly provides a better estimate to L than the Wiedemann-Franz law. At higher S, the discrepancy becomes more pronounced as our predicted L significantly decreases and reaches an asymptotic value at high Seebeck of around 10^{-8} WΩ K^{-2}.

IV. CONCLUSION

We have presented a detailed analysis of the thermoelectric coefficients of n-doped silicon via the exact solution of the linearized Boltzmann transport equation for electrons, also accounting for the effect of nonequilibrium phonon populations induced by a temperature gradient. We have discussed electron mobility, the Lorenz number, and the Seebeck coefficient in a range of temperatures and carrier concentrations. The theoretical results compare reasonably well with the available experimental data and provide a detailed characterization of the relative importance of the different scattering mechanisms. We have also analyzed the accuracy of different flavors of relaxation time approximations, as well as of a simplified model to extract the Lorenz number from experimental data. The computational approach that we have implemented is very general and can be applied to doped semiconductors as well to metallic systems. We believe that along this route more compounds will be systematically studied to gain a detailed microscopic understanding of their thermoelectric transport properties.

ACKNOWLEDGMENTS

N.B. acknowledges support from EU FP7/CIG (Grant No. 294158).

APPENDIX A: PERFORMANCE AND ACCURACY OF THE BE SOLVER

In order to solve the linear equation $\boldsymbol{Ax} = \boldsymbol{b}$, we use the preconditioned conjugate gradient method [33], where the diagonal of A is used as preconditioner. The performance of the CG algorithm is shown in Fig. 11: the CG converges in 6 or 7 iterations, while with the addition of the preconditioning an accurate solution is obtained already after 2–3 iterations. In our experience standard iterative approaches [49] converge very slowly, especially in the presence of charged impurity scattering.

In order to assess the accuracy of the solution of the BE, it is interesting to numerically verify the validity of the Kelvin relation, $\sigma S = \alpha / T$. The lower panel of Fig. 11 shows that, when phonons are in thermal equilibrium, the converged solutions of the BE's with temperature gradient and electric field as driving forces satisfy the Kelvin relation; the CG algorithm with preconditioning produces the converged result extremely quickly. In passing, it is worth mentioning that, as shown in Ref. [50], the Kelvin relations are satisfied also when the departure from equilibrium of both electron and phonon distribution functions is taken into account. In this work, however, we are not in the position to be able to verify directly this result as we have neglected the effect of the electrons on the phonon transport, an appropriate assumption only at low doping.

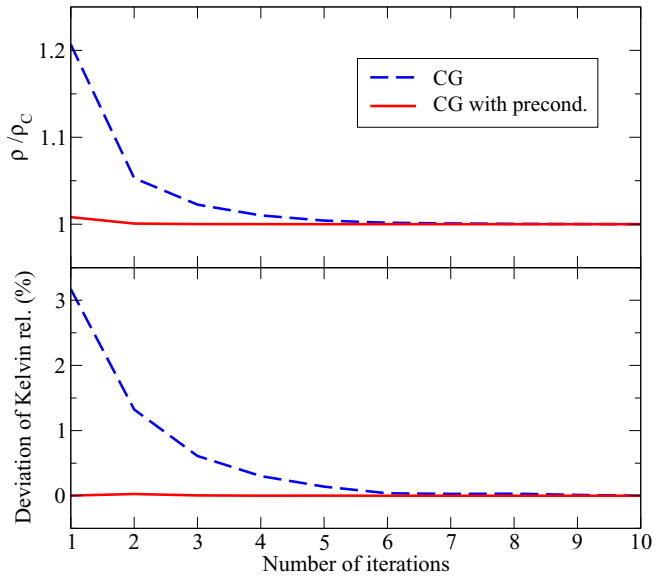

FIG. 11. Performance of the CG algorithm. (Top) Resistivity (normalized to the converged result ρ_C) as a function of the number of iterations. (Bottom) Deviation from the Kelvin relation as a function of the number of iterations. The dashed blue (solid red) line is the result of the CG (with preconditioning). The results are for $n = 1.75 \times 10^{14}$ cm^{-3}, $T = 300$ K and with phonons in thermal equilibrium.

The BE solver implemented in this work has been fully parallelized for use on distributed memory clusters so that the collision matrix $\boldsymbol{A}$, that scales quadratically with the number of electronic states, can be decomposed among the processes. An efficient way to tile the matrix is the *chessboard* fashion, by defining an MPI cartesian topology in which each process is given a tile of the matrix. The main advantage of the cartesian topology is that loading the collision matrix can be efficiently distributed, reducing greatly time and memory consumption.

APPENDIX B: SAMPLING OF THE BRILLOUIN ZONE

Here, we discuss the choice of the numerical parameters used to compute the transport coefficients. These parameters are (i) the mesh $N_{\mathrm{EPC}} \times N_{\mathrm{EPC}} \times N_{\mathrm{EPC}}$ of k points on which we compute the electron-phonon coupling matrix elements via Wannier interpolation, (ii) the fine grid $N_f \times N_f \times N_f$ (where we use $N_f = p\, N_{\mathrm{EPC}}$, with $p = 1$, 2, and 3) used to solve the BE and compute the transport quantities, (iii) the energy window from the bottom of the conduction band used to restrict the number of k points, and (iv) the width σ_g of the Gaussians used to replace the delta functions in the transition probabilities.

In Fig. 12, we present the electron mobility as a function of the number of k-points used to solve the BE. The different symbols correspond to different values for N_{EPC}, p, and σ_g. Our results shows that even with a $N_{\mathrm{EPC}} = 110$ and $p = 1$ (that is very computationally demanding) the convergence is not yet fully achieved. However, increasing the effective mesh with $p = 2$ and $p = 3$ gives stable mobilities, even when starting from different N_{EPC} (i.e., $N_{\mathrm{EPC}} = 70$,90), which implies that

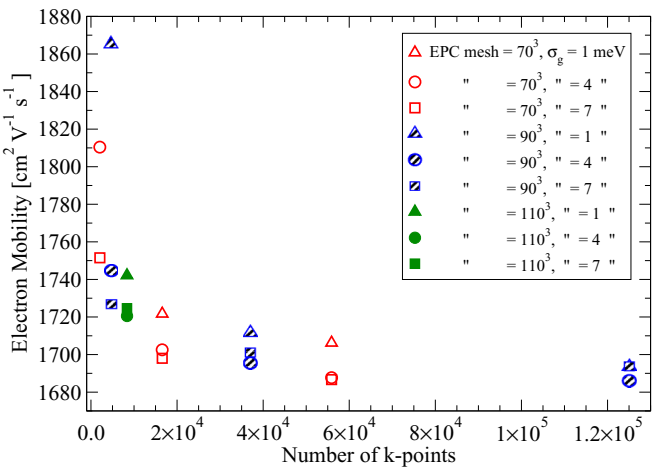

FIG. 12. Electron mobility at room temperature and for $n = 1.6 \times 10^{15}$ cm^{-3} as a function of the number of k points used to solve the BE. Different electron-phonon coupling grids are used: $N_{\mathrm{EPC}} = 70$ (red empty symbols), 90 (blue patterned symbols), and 110 (green full symbols). The values of σ_g used are 1 (triangles), 4 (circles), and 7 meV (squares). The results obtained with less (more) than 10^4 (5×10^4) k points on the x axis are for $p = 1$ ($p = 3$); the remaining points are for $p = 2$. The energy window used is 0.15 eV.

the electron-phonon matrices are accurately sampled already with these meshes.

The choice of the energy window to select the states relevant for transport depends on the thermoelectric transport coefficients under consideration. While a window of 0.15 eV is sufficient to obtain converged results for the electron mobility [51], other coefficients require a larger window. For instance, Fig. 13 clearly shows that the accurate evaluation of the Seebeck coefficient requires an energy window considerably smaller than the one needed to compute the Lorenz number. In addition, the energy window might also depend slightly on the relevant scattering mechanisms. It is possible to see this for the Lorenz number (a quantity that is much more sensitive than the Seebeck coefficient to the scattering mechanisms included in the BE): when only impurity scattering is considered there is large contribution from electronic states quite far from the bottom of the conduction band and the energy window required for the convergence is slightly larger than in the case in which only phonon scattering is included.

APPENDIX C: APPROXIMATE APPROACHES

Figure 14 compares different approximate approaches within the BE framework to estimate the phonon-limited electron mobility at low doping. A popular approach is the relaxation time approximation (RTA) in which a relaxation time is computed using the formula

$$\frac{1}{\tau^{\mathrm{RTA}}_{m\boldsymbol{k}}} = \frac{2\pi}{\hbar}\frac{1}{N_{\boldsymbol{q}}}\sum_{m',\lambda,\boldsymbol{q}} \left|g^{\lambda}_{mm'}(\boldsymbol{k};\boldsymbol{q})\right|^2 \times \left\{\left[f^0_{m'}(\boldsymbol{k}+\boldsymbol{q}) + n^0_{\lambda}(\boldsymbol{q})\right]\delta[\epsilon_{m'\boldsymbol{k}+\boldsymbol{q}} - \epsilon_{m\boldsymbol{k}} - \hbar\omega_{\lambda}(\boldsymbol{q})] + \left[1 + n^0_{\lambda}(\boldsymbol{q}) - f^0_{m'}(\boldsymbol{k}+\boldsymbol{q})\right]\delta[\epsilon_{m'\boldsymbol{k}+\boldsymbol{q}} - \epsilon_{m\boldsymbol{k}} + \hbar\omega_{\lambda}(\boldsymbol{q})]\right\}, \quad \text{(C1)}$$

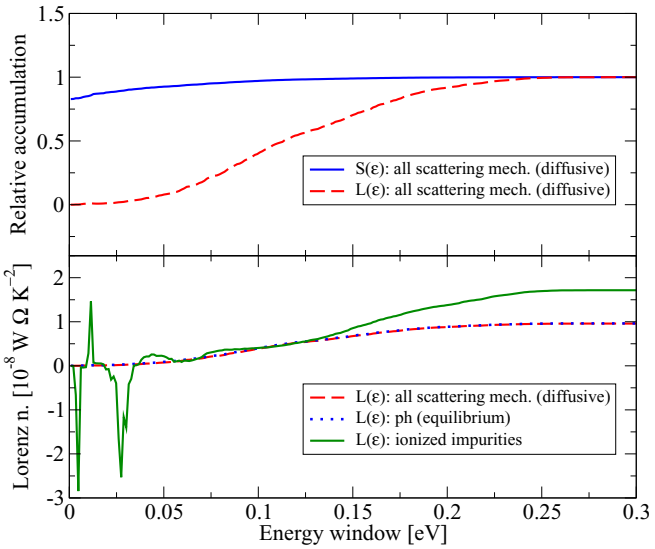

FIG. 13. L and S as a function of the energy window used to compute the integrals of the transport coefficients in Eq. (7). (Top) Relative accumulation of S (solid blue line) and L (dashed red line) computed under the assumption of phonons in thermal equilibrium. (Bottom) L as a function of the energy window for different scattering mechanisms. Dashed red line corresponds to L computed with all scattering terms, while the solid green line (dotted blu line) is for the impurity (phonon) contribution. In all cases, the BE at room temperature and for $n = 10^{14}$ cm^{-3} is solved for all the states up to 0.32 eV above the bottom of the conduction band.

and it is then used in Eq. (7) to compute the transport coefficients. As shown in Fig. 14, this approach gives mobilities that are around 4%–5% lower than the exact solution of the BE. It

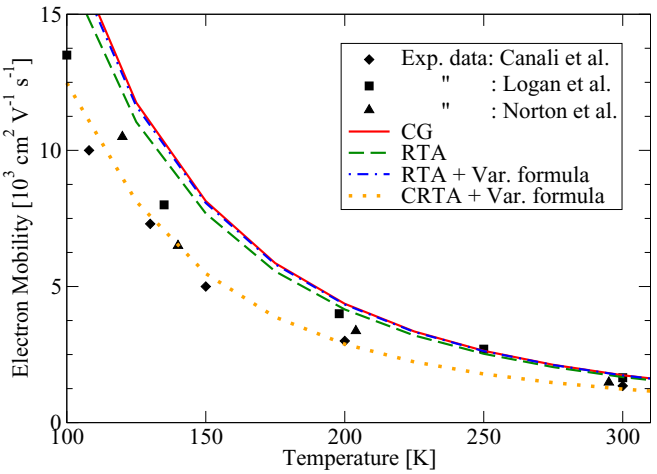

FIG. 14. Intrinsic electron mobility as a function of temperature computed with different approaches: the solid red line is from solution of the BE (CG), the dashed green line is the relaxation time approximation (RTA), the dot-dashed blu line (dotted orange line) is obtained using $\chi_m(\boldsymbol{k}) \propto v_m^{||}(\boldsymbol{k})\tau_{m\boldsymbol{k}}^{\mathrm{RTA}}$ ($\chi_m(\boldsymbol{k}) \propto v_m^{||}(\boldsymbol{k})$) as a trial function in the variational formula Eq. (14). The symbols are the experimental data as in Fig. 2.

is interesting to use $\chi_m(\boldsymbol{k}) \propto v_m^{||}(\boldsymbol{k})\tau_{m\boldsymbol{k}}^{\mathrm{RTA}}$ as a trial function in the variational formula for the resistivity, Eq. (14). Also in this case, the mobility is lower than the exact result (because of the variational principle), but now the difference with respect to the exact result is less than 1%. A simpler approach, in which the trial function is only proportional to the velocity gives results that are fortuitously close to the experimental results but much lower than the result obtained from the exact solution of the BE.

[1] M. Zebarjadi, K. Esfarjani, M. S. Dresselhaus, Z. F. Ren, and G. Chen, Energy Environ. Sci. **5**, 5147 (2012).
[2] B. Xu and M. J. Verstraete, Phys. Rev. Lett. **112**, 196603 (2014).
[3] Z. Wang, S. Wang, S. Obukhov, N. Vast, J. Sjakste, V. Tyuterev, and N. Mingo, Phys. Rev. B **83**, 205208 (2011).
[4] W. Li, Phys. Rev. B **92**, 075405 (2015).
[5] N. Marzari, A. A. Mostofi, J. R. Yates, I. Souza, and D. Vanderbilt, Rev. Mod. Phys. **84**, 1419 (2012).
[6] F. Giustino, M. L. Cohen, and S. G. Louie, Phys. Rev. B **76**, 165108 (2007).
[7] C. Jacoboni and L. Reggiani, Rev. Mod. Phys. **55**, 645 (1983).
[8] O. D. Restrepo, K. Varga, and S. T. Pantelides, Appl. Phys. Lett. **94**, 212103 (2009).
[9] F. Murphy-Armando and S. Fahy, Phys. Rev. B **78**, 035202 (2008).
[10] B. Qiu, Z. Tian, A. Vallabhaneni, B. Liao, J. M. Mendoza, O. D. Restrepo, X. Ruan, and G. Chen, Europhys. Lett. **109**, 57006 (2015).
[11] J. Zhou, B. Liao, B. Qiu, S. Huberman, K. Esfarjani, M. S. Dresselhaus, and G. Chen, Proc. Natl. Acad. Sci. USA **112**, 14777 (2015).
[12] G. D. Mahan, L. Lindsay, and D. A. Broido, J. Appl. Phys. **116**, 245102 (2014).
[13] J. Sadhu, H. Tian, J. Ma, B. Azeredo, J. Kim, K. Balasundaram, C. Zhang, X. Li, P. M. Ferreira, and S. Sinha, Nano Lett. **15**, 3159 (2015).
[14] T. H. Geballe and G. W. Hull, Phys. Rev. **98**, 940 (1955).
[15] C. Herring, Phys. Rev. **96**, 1163 (1954).
[16] J. Ziman, *Electrons and Phonons: The Theory of Transport Phenomena in Solids*, International Series of Monographs on Physics (OUP Oxford, Oxford, 1960).
[17] N. A. Mecholsky, L. Resca, I. L. Pegg, and M. Fornari, Phys. Rev. B **89**, 155131 (2014).
[18] G. D. Mahan and J. O. Sofo, Proc. Natl. Acad. Sci. USA **93**, 7436 (1996).
[19] V. Lordi, P. Erhart, and D. Åberg, Phys. Rev. B **81**, 235204 (2010).
[20] B. Ridley, *Quantum Processes in Semiconductors*, Oxford Science Publications (OUP Oxford, Oxford, 1999).
[21] L. Gurevich, J. Phys. (Moscow) **9**, 477 (1945).
[22] H. Frederikse, Phys. Rev. **92**, 248 (1953).
[23] T. Geballe and G. Hull, Phys. Rev. **94**, 1134 (1954).
[24] D. Cantrell and P. Butcher, J. Phys. C **20**, 1985 (1987).
[25] B. Liao, B. Qiu, J. Zhou, S. Huberman, K. Esfarjani, and G. Chen, Phys. Rev. Lett. **114**, 115901 (2015).

[26] P. Giannozzi, S. Baroni, N. Bonini, M. Calandra, R. Car, C. Cavazzoni, D. Ceresoli, G. L. Chiarotti, M. Cococcioni, I. Dabo, A. D. Corso, S. de Gironcoli, S. Fabris, G. Fratesi, R. Gebauer, U. Gerstmann, C. Gougoussis, A. Kokalj, M. Lazzeri, L. Martin-Samos, N. Marzari, F. Mauri, R. Mazzarello, S. Paolini, A. Pasquarello, L. Paulatto, C. Sbraccia, S. Scandolo, G. Sclauzero, A. P. Seitsonen, A. Smogunov, P. Umari, and R. M. Wentzcovitch, J. Phys.: Condens. Matter **21**, 395502 (2009).
[27] J. P. Perdew and A. Zunger, Phys. Rev. B **23**, 5048 (1981).
[28] A. A. Mostofi, J. R. Yates, Y.-S. Lee, I. Souza, D. Vanderbilt, and N. Marzari, Comput. Phys. Commun. **178**, 685 (2008).
[29] J. Noffsinger, F. Giustino, B. D. Malone, C.-H. Park, S. G. Louie, and M. L. Cohen, Comput. Phys. Commun. **181**, 2140 (2010).
[30] C.-H. Park, N. Bonini, T. Sohier, G. Samsonidze, B. Kozinsky, M. Calandra, F. Mauri, and N. Marzari, Nano Lett. **14**, 1113 (2014).
[31] B. Liao, J. Zhou, B. Qiu, M. S. Dresselhaus, and G. Chen, Phys. Rev. B **91**, 235419 (2015).
[32] A. Jain and A. J. H. McGaughey, Phys. Rev. B **93**, 081206 (2016).
[33] A. Greenbaum, *Iterative Methods for Solving Linear Systems*, Frontiers in Applied Mathematics (Society for Industrial and Applied Mathematics, Philadelphia, 1997).
[34] G. Fugallo, M. Lazzeri, L. Paulatto, and F. Mauri, Phys. Rev. B **88**, 045430 (2013).
[35] J. Garg, N. Bonini, B. Kozinsky, and N. Marzari, Phys. Rev. Lett. **106**, 045901 (2011).
[36] J. Garg, N. Bonini, and N. Marzari, in *Length-scale Dependent Phonon Interactions*, edited by S. Shinde and G. Srivastava, Topics in Applied Physics Vol. 128 (Springer, New York, 2014), pp. 115–136.
[37] C. Jacoboni, C. Canali, G. Ottaviani, and A. A. Quaranta, Solid-State Electron. **20**, 77 (1977).
[38] G. Antonius, S. Poncé, P. Boulanger, M. Côté, and X. Gonze, Phys. Rev. Lett. **112**, 215501 (2014).
[39] M. V. Fischetti, Phys. Rev. B **44**, 5527 (1991).
[40] C. Canali, C. Jacoboni, F. Nava, G. Ottaviani, and A. Alberigi-Quaranta, Phys. Rev. B **12**, 2265 (1975).
[41] R. A. Logan and A. J. Peters, J. Appl. Phys. **31**, 122 (1960).
[42] P. Norton, T. Braggins, and H. Levinstein, Phys. Rev. B **8**, 5632 (1973).
[43] F. Mousty, P. Ostoja, and L. Passari, J. Appl. Phys. **45**, 4576 (1974).
[44] G. K. H. Madsen and D. J. Singh, Comput. Phys. Commun. **175**, 67 (2006).
[45] G. Pizzi, D. Volja, B. Kozinsky, M. Fornari, and N. Marzari, Comput. Phys. Commun. **185**, 422 (2014).
[46] P. Pichanusakorn and P. Bandaru, Mater. Sci. Eng., R **67**, 19 (2010).
[47] E. Flage-Larsen and Ø. Prytz, Appl. Phys. Lett. **99**, 202108 (2011).
[48] H.-S. Kim, Z. M. Gibbs, Y. Tang, H. Wang, and G. J. Snyder, Appl. Phys. Lett. Mat. **3**, 041506 (2015).
[49] F. X. Bronold, in *Computational Many-Particle Physics*, edited by H. Fehske, R. Schneider, and A. Weisse, Lecture Notes in Physics Vol. 739 (Springer-Verlag Berlin, Germany, 2008), pp. 223–254.
[50] E. H. Sondheimer, Proc. R. Soc. London A **234**, 391 (1956).
[51] This energy window includes also the contribution of the second conduction band that starts at around 0.13 eV from the bottom of the conduction band.